Electronic Supplementary Information

Photo-responsive dimension-controlled ion-pairing assemblies based on anion complexes of π-electronic systems

Ryohei Yamakado, Yohei Haketa, Mitsuo Hara, Shusaku Nagano, Takahiro Seki and Hiromitsu Maeda*

Department of Organic Materials Science, Graduate School of Organic Materials Science, Yamagata University, Yonezawa 992–8510, Japan, Department of Applied Chemistry, College of Life Sciences, Ritsumeikan University, Kusatsu 525–8577, Japan, Fax: +81 77 561 2659; Tel: +81 77 561 5969; E-mail: maedahir@ph.ritsumei.ac.jp, Department of Molecular and Macromolecular Chemistry, Graduate School of Engineering, Nagoya University, Nagoya 464–8603, Japan, and Nagoya University Venture Business Laboratory, Nagoya 464–8603, Japan

Table of Contents

1. Synthetic procedure and spectroscopic data

General procedures. Starting materials was purchased from Kanto Chemical Co., Nacalai Tesque Inc., TCI Chemical Co., and FUJIFILM Wako Pure Chemical Co., and used without further purification unless otherwise stated. All reactions were performed under dry nitrogen atmosphere unless otherwise noted. NMR spectra used in the characterization of products were recorded on a JEOL JNM-ECZ-600R/M1 600 MHz spectrometer. All NMR spectra were referenced to solvent. UV-visible absorption spectra were recorded on a JASCO V-570. TLC analyses were carried out on aluminum sheets coated with silica gel 60 (Merck 5554).

Ethyl 6-[4-(4-dodecyloxyphenylazo)phenoxy]-hexanoate, 3. Ethyl 4-bromobutyrate (560 µL, 3.9 mmol) was added to a solution of 4-[2-(4-dodecyloxyphenyl)diazenyl]phenol[S1] (500 mg, 1.3 mmol) and K_2CO_3 (250 mg, 1.8 mmol) in acetone (20 mL) at 60 °C, and the mixture was stirred overnight. The solvent was evaporated under vacuum, and recrystallization from *n*-hexane afforded **3** (466 mg, 2.34 mmol, 77%) as a yellow solid. ^{1}H NMR (600 MHz, $CDCl_3$, 20 °C): δ (ppm) 7.85 (d, J = 9.0 Hz, 4H, Ar-H), 6.98 (d, J = 9.0 Hz, 2H, Ar-H), 6.97 (d, J = 9.0 Hz, 2H, Ar-H), 4.14 (q, J = 7.2 Hz, 2H, $CO_2CH_2CH_3$), 4.02 (m, OCH_2, 4H), 2.34 (t, J = 7.8 Hz, 2H, $CH_2CO_2C_2H_5$), 1.83 (m, 4H, OCH_2CH_2), 1.72 (m, 2H, $CH_2CH_2CO_2C_2H_5$), 1.53 (m, 2H, $CH_2(CH_2)_2CO_2C_2H_5$), 1.53 (m, 2H, $O(CH_2)_2CH_2$), 1.36 (m, 2H, $O(CH_2)_3CH_2$), 1.87–1.20 (m, 17H, $O(CH_2)_4(CH_2)_7$ + $CO_2CH_2CH_3$), 0.88 (t, J = 7.2 Hz, 3H, $O(CH_2)_{11}CH_3$). ^{13}C NMR (151 MHz, $CDCl_3$, 20 °C): δ (ppm) 173.63, 161.17, 161.00, 146.96, 124.28, 114.64, 114.61, 68.32, 67.92, 60.27, 34.23, 31.91, 29.65, 29.57, 29.38, 29.34, 29.20, 28.89, 26.01, 24.69, 22.68, 14.25, 14.12 (some signals were overlapped). MALDI-TOF-MS: *m/z* (% intensity): 525.4 (100). Calcd for $C_{32}H_{49}N_2O_4$ ([M + H]$^+$): 525.37.

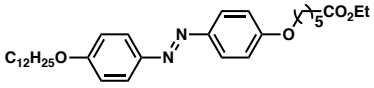

6-[4-(4-Dodecyloxyphenylazo)phenoxy]hexanoic acid, 4. [S2] KOH (300 mg, 5.4 mmol) was added to a solution of **3** (580 mg, 1.1 mmol) in THF (3 mL) and H_2O (3 mL) at 70 °C, and the mixture was stirred overnight. The reaction mixture was cooled to rt, and the solution was acidified with a dilute HCl aqueous solution. The precipitation was collected by filtration to afford **4** (465 mg, 0.94 mmol, 85%) as an orange solid. ^{1}H NMR (600 MHz, DMSO-d_6, 20 °C): δ (ppm) 7.81 (d, J = 9.0 Hz, 4H, Ar-H), 7.10 (d, J = 9.0 Hz, 4H, Ar-H), 4.06 (t, J = 6.0 Hz, 4H, OCH_2), 2.24 (t, J = 7.2 Hz, 2H, CH_2CO_2H), 1.74 (t, J = 6.0 Hz, 4H, OCH_2CH_2), 1.56 (t, J = 7.2 Hz, 2H, $CH_2CH_2CO_2H$), 1.43 (m, 4H, $O(CH_2)_2CH_2$), 1.33 (m, 2H, $O(CH_2)_3CH_2$), 1.30–1.21 (m, 14H, $O(CH_2)_4(CH_2)_7$), 0.85 (t, J = 7.2 Hz, 3H, $O(CH_2)_{11}CH_3$). ^{13}C NMR (151 MHz, DMSO-d_6, 20 °C): δ (ppm) 174.46, 160.90, 146.09, 124.12, 114.96, 67.82, 33.62, 31.30, 29.03, 28.98, 28.73, 28.58, 28.36, 25.45, 25.12, 24.27, 22.11, 13.97 (some signals were overlapped). MALDI-TOF-MS: *m/z* (% intensity): 495.3 (100). Calcd for $C_{30}H_{43}N_2O_4$ ([M – H]$^-$): 495.32.

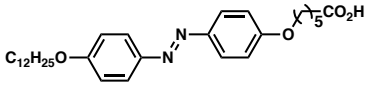

Tetrabutylammonium 6-[4-(4-dodecyloxyphenylazo)-phenoxy]hexanoate, 4$^-$-TBA$^+$. TBAOH (37% in MeOH) (70 µL, 0.10 mmol) was added to a solution of **4** (49.7 mg, 0.10 mmol) in THF (3 mL) at rt. The mixture was stirred for 10 min, and the solvent was evaporated under vacuum. Recrystallization from EtOAc/*n*-hexane afforded **4**$^-$-TBA$^+$ (29.6 mg, 0.040 mmol, 40%) as an orange solid. ^{1}H NMR (600 MHz, $CDCl_3$, 20 °C): δ (ppm) 7.85 (d, J = 9.0 Hz, 2H, Ar-H), 7.84 (d, J = 9.0 Hz, 2H, Ar-H), 6.99 (d, J = 9.0 Hz, 2H, Ar-H), 6.97 (d, J = 9.0 Hz, 2H, Ar-H), 4.02 (t, J = 7.2 Hz, 4H, OCH_2), 3.36 (t, J = 7.2 Hz, 8H, NCH_2), 2.22 (t, J = 7.2 Hz, 2H, $CH_2CO_2^-$), 1.87–1.20 (m, 42H, $OCH_2(CH_2)_{10}$ + $(CH_2)_3CH_2CO_2^-$ + $NCH_2(CH_2)_2$), 1.00 (t, J = 7.2 Hz, 12H, $N(CH_2)_3CH_3$), 0.88 (t, J = 7.2 Hz, 3H, $O(CH_2)_{11}CH_3$). ^{13}C NMR (151 MHz, $CDCl_3$, 20 °C): δ (ppm) 179.39, 161.08, 146.92, 124.23, 114.66, 68.46, 68.30, 58.73, 39.11, 31.89, 29.63, 29.57, 29.19, 26.28, 24.00, 22.66, 19.72, 14.10, 13.68 (some signals were overlapped). UV/vis (CH_2Cl_2, λ_{max}[nm] (ε, 10^4 $M^{-1}cm^{-1}$)): 361 (3.3).

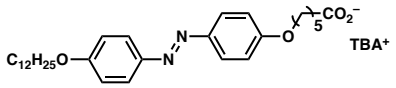

[S1] L. A. Benedini, M. A. Sequeira, M. L. Fanani, B Maggio and V. Dodero, *J. Phys. Chem. B*, 2016, **120**, 4053–4063.

[S2] Y. Kageyama, T. Ikegami, Y. Kurokome and S. Takeda, *Chem. Eur. J.*, 2016, **22**, 8669–8675.

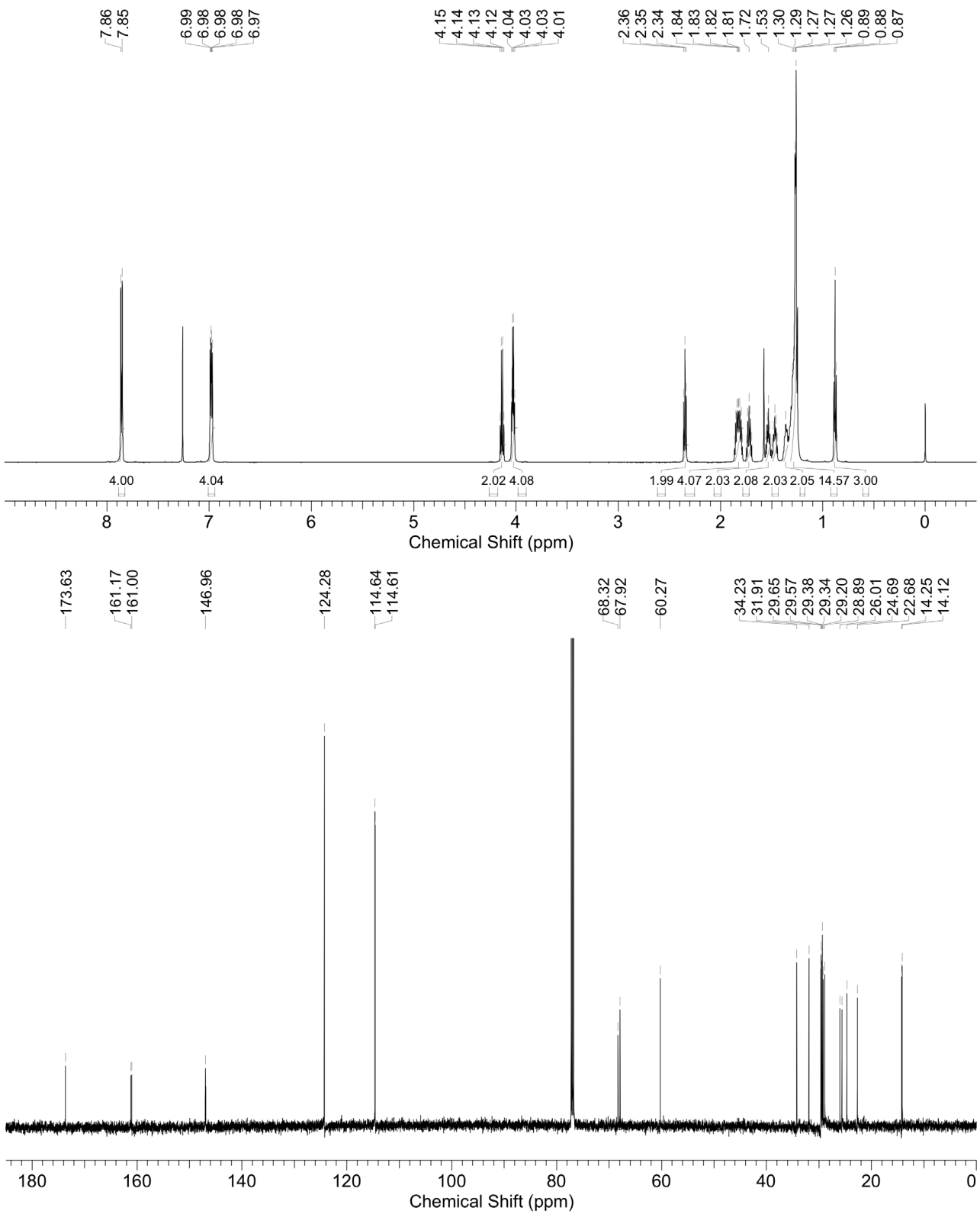

Fig. S1 ^{1}H NMR (top) and ^{13}C NMR (bottom) spectra of **3** in $CDCl_3$.

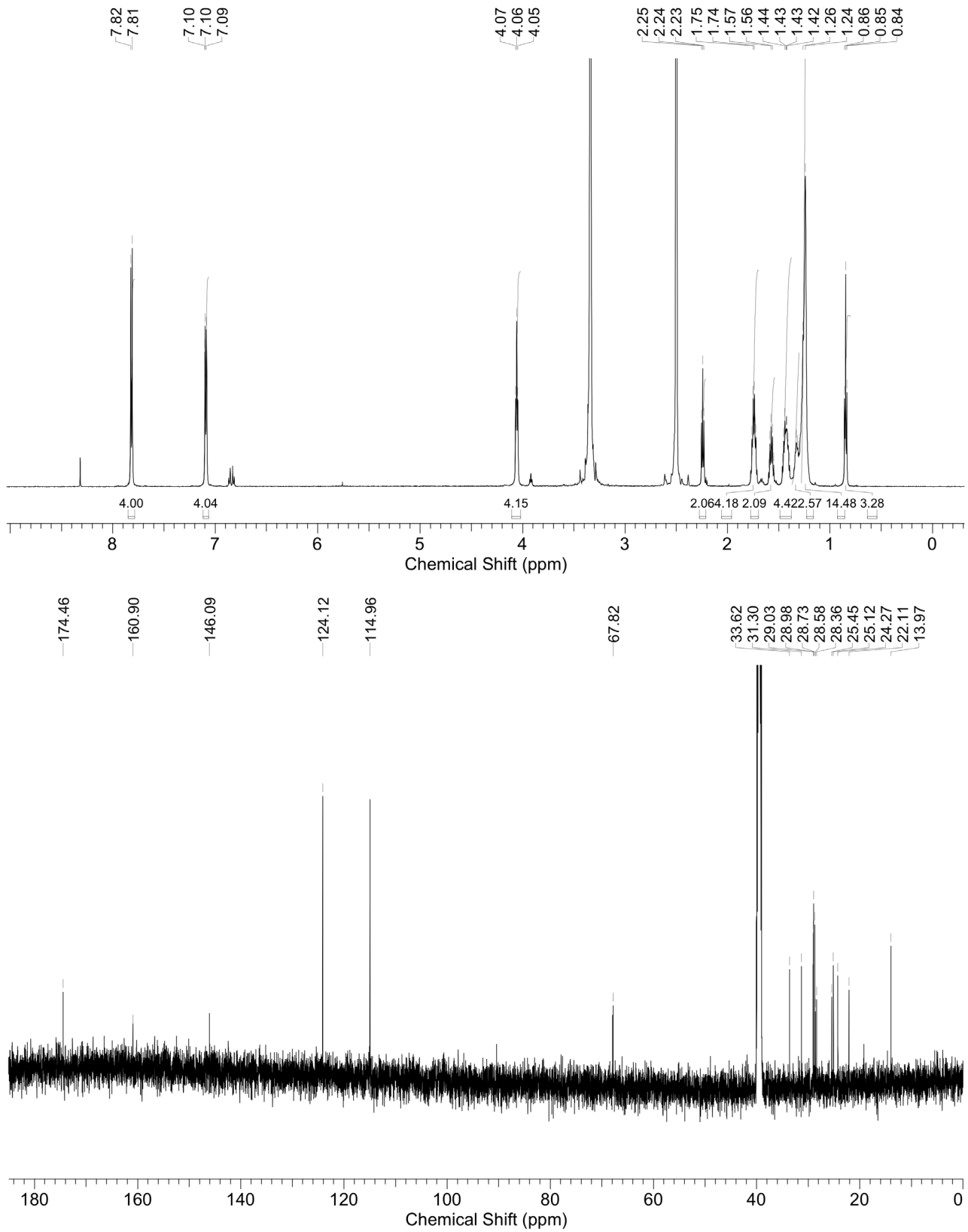

Fig. S2 ^{1}H NMR (top) and ^{13}C NMR (bottom) spectra of **4** in DMSO-d_6.

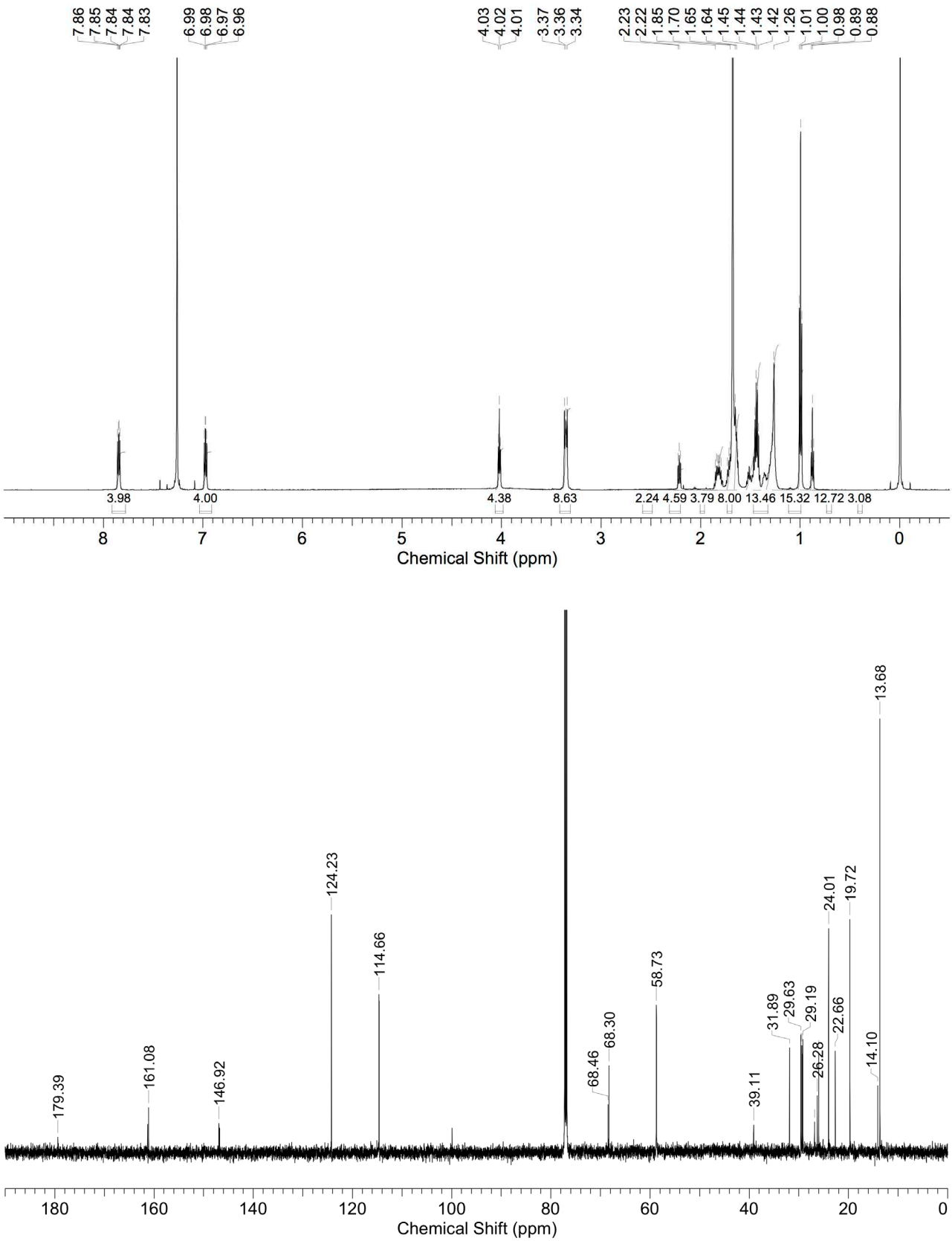

Fig. S3 ^{1}H NMR (top) and ^{13}C NMR (bottom) spectra of **4**$^{-}$-TBA^{+} in $CDCl_3$.

2. Anion-binding behaviors

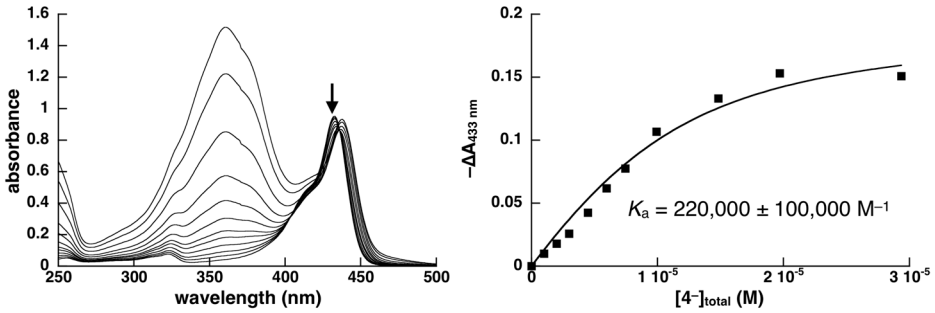

Fig. S4 UV/vis absorption spectral change (left) and corresponding titration plot and 1:1 fitting curve (right) of **2a** (1.0×10^{-5} M) upon the addition of $\mathbf{4}^{-}$-TBA^{+} in CH_2Cl_2. The error of the binding constant was slightly large probably because of the absorption of $\mathbf{4}^{-}$.

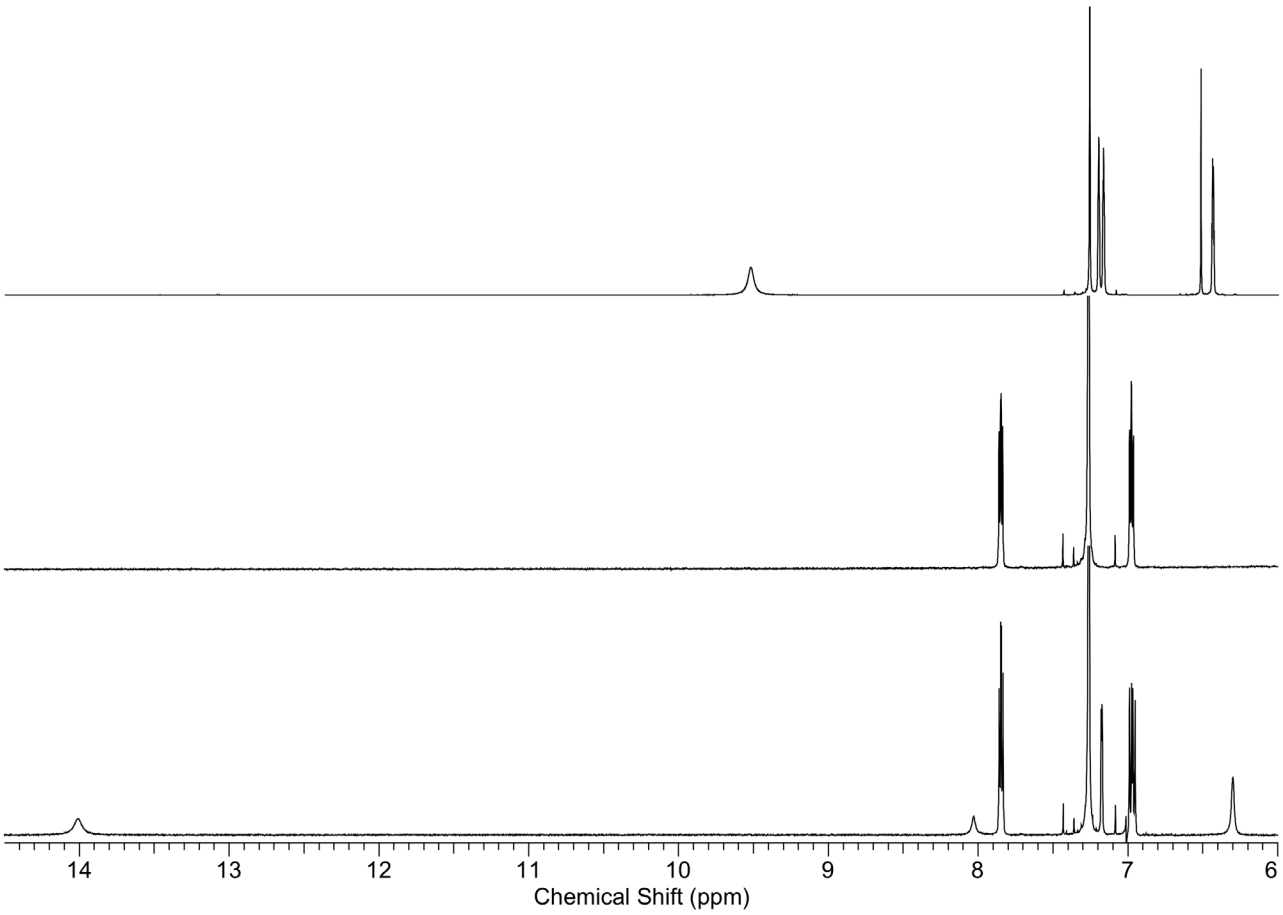

Fig. S5 ^1H NMR spectra of **2a** (top), $\mathbf{4}^{-}$-TBA^{+} (middle), and $\mathbf{2a}\cdot\mathbf{4}^{-}$-$TBA^{+}$ (bottom) in $CDCl_3$.

3. Theoretical study

DFT calculations. DFT calculations of the geometrical optimization were carried out by Gaussian 09 program.[S3]

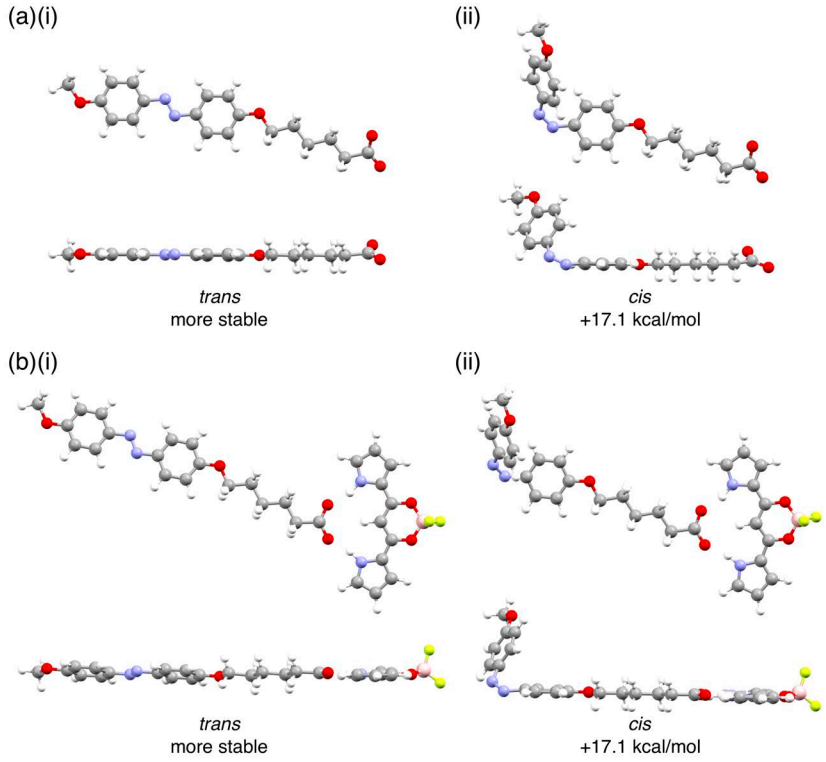

Figure S6 Optimized structures (top and side views) of (a)(i) *trans*-**4′**$^{-}$ and (ii) *cis*-**4′**$^{-}$ and (b)(i) **2a**·*trans*-**4′**$^{-}$ and (ii) **2a**·*cis*-**4′**$^{-}$ calculated at B3LYP/6-31+G(d,p) level of theory with methoxy groups replacing the dodecyloxy groups for facile calculations.

Cartesian Coordination of *trans*-4′$^{-}$
-1147.16198 hartree
C,3.1608165533,1.1399877012,-0.2374025786
C,1.6933632123,1.6606148838,-0.4401108268
C,0.6024663792,0.749787076,0.1272423258
C,-0.8233825881,1.1895407184,-0.2372239076
C,-1.9128823987,0.2769280713,0.348078378
C,-3.3100136334,0.7404452111,-0.0279174623
C,-5.5927357352,0.0560713986,0.3660396755
C,-6.1315860541,1.1237131861,-0.371281155
C,-6.4625198688,-0.8815787143,0.9689891379
C,-7.5158655362,1.2410881834,-0.4942888698
C,-7.8330280455,-0.7570238929,0.8406012554
C,-8.3824889217,0.3146461136,0.1013092874
C,-11.9138808099,-0.0522198071,0.2319208331
C,-12.7949515139,-0.9765283073,0.8035975098
C,-12.4441495111,1.0374437525,-0.4910310186
C,-14.1794114076,-0.8381765243,0.6698850147
C,-13.8145892578,1.1831998837,-0.6285452061
C,-14.6929530379,0.2472664283,-0.049850132
H,1.5487070129,1.7738037998,-1.5266666251
H,1.6245823101,2.6708351858,-0.0156281106
H,0.7896379485,-0.2706223132,-0.2268295139
H,0.6988986357,0.707236934,1.2218276568
H,-0.989591726,2.2215363784,0.108878964
H,-0.9222624446,1.2167667757,-1.3333241137
H,-1.7692299373,-0.7512732062,-0.0067688126
H,-1.8298818889,0.2493164652,1.441977134
H,-3.4996292176,1.7553879107,0.3471786614
H,-3.4427665553,0.7430935811,-1.1183824527
H,-5.4874298199,1.8542500466,-0.8442065062
H,-6.0208266878,-1.697368629,1.5326075909
H,-7.9485020578,2.0608180366,-1.0601339069
H,-8.5006016042,-1.4754927259,1.3024659673
H,-12.3775458195,-1.8113890238,1.3583172391
H,-11.7628186768,1.754788271,-0.9339679456
H,-14.2385359933,2.0160660504,-1.1810254088
H,-14.8339896176,-1.571793887,1.1250978674
N,-9.7576587446,0.5420424039,-0.0949379167
N,-10.5360196107,-0.2985130254,0.4370133982
O,4.0513398393,2.0299902126,-0.2881553846
O,3.292774497,-0.1044784278,-0.0787297221
O,-4.2735737566,-0.1620330683,0.5571736057
O,-16.025064636,0.4870677236,-0.2470026844
C,-16.9674589056,-0.4191404084,0.3101038322
H,-17.9500230582,-0.0362230026,0.0308380445
H,-16.8411004144,-1.4297949507,-0.0985492382
H,-16.8887646656,-0.4563295694,1.4040988598

Cartesian Coordination of *cis*-4′$^{-}$
-1147.1347897 hartree
C,-2.7376222775,-1.1574098993,-0.3482623919

C,-1.3387071855,-1.8682117489,-0.2879326178
C,-0.1760232162,-0.9621456314,0.1231690977
C,1.2040291827,-1.6225356195,-0.012574393
C,2.3630311649,-0.7080630946,0.4152311142
C,3.7144452915,-1.3832779378,0.2538435551
H,-1.1492743679,-2.2718724534,-1.2957087742
H,-1.4205851667,-2.7355441291,0.3800588557
H,-0.2242045497,-0.0502451314,-0.4832973854
H,-0.3197640426,-0.6366298011,1.1638228685
H,1.2312712402,-2.5466465906,0.5853700223
H,1.3523748991,-1.9323501115,-1.0585059541
H,2.3505455224,0.2133228397,-0.1802921951
H,2.2369905477,-0.4095877326,1.4636993296
H,3.7726586074,-2.2946119037,0.8647123824
H,3.8922039627,-1.6569380189,-0.7952389132
O,-3.7294729457,-1.9230778623,-0.2160068024
O,-2.7196548371,0.0871943375,-0.5535458209
O,4.746022034,-0.4677300956,0.6796526909
C,6.042167461,-0.8455747702,0.6068949242
C,6.4904578739,-2.0990162959,0.1571341548
C,6.9861059375,0.107447949,1.0425240822
C,7.8570872148,-2.3785480967,0.1506737507
H,5.7882426256,-2.860267128,-0.1589542611
C,8.343753925,-0.1633181245,0.9888945184
H,6.6198582346,1.0569213724,1.4195782471
C,8.802281432,-1.4113514813,0.5166691289
H,8.2122362241,-3.3589589204,-0.1528405032
H,9.0491697512,0.5848562398,1.3312261743
N,10.1585636658,-1.8564033278,0.5481152022
N,11.1581599696,-1.1348756786,0.3124639923
C,11.0926354937,0.1842837898,-0.2459855022
C,11.9846545068,1.1327356287,0.2626330324
C,10.3444333115,0.5034176743,-1.3958328075
C,12.0826680635,2.4084665342,-0.3013719884
H,12.6009919201,0.8658179946,1.1160391673
C,10.4645180406,1.7537412311,-1.9855171864
H,9.6748311995,-0.2317524611,-1.8285399253
C,11.3206090841,2.7218396831,-1.4336663795
H,12.7648857733,3.1289227463,0.1338641767
H,9.8987651174,2.0071139661,-2.8763572614
O,11.3513418072,3.9263988187,-2.0820235946
C,12.1900199933,4.9517409694,-1.5682898281
H,12.0438827916,5.8118939022,-2.2230604939
H,11.9083081644,5.2233484695,-0.5428833289
H,13.2463937243,4.6541417597,-1.5891253896

Cartesian Coordination of 2a·*trans*-4′⁻

-2056.5619063 hartree

B,9.6467727934,-1.1290475689,-0.2525447067
C,7.8412428206,2.1352800937,-0.1246894832
C,8.0275747227,0.707063848,-0.1117161148
C,6.9694506084,-0.20869277,-0.1326415809
C,7.2496926458,-1.571804735,0.0123361258
C,6.2305617135,-2.5831905743,0.131320474
C,8.8167228672,3.1407331829,-0.1306191268
C,8.1433493234,4.377410994,-0.1432943315
C,6.7755620898,4.0920423232,-0.1453857849
C,4.1924085426,-3.4739225581,0.2697523537
C,5.1009079401,-4.5333985807,0.330051235
C,6.3888828403,-3.9703476705,0.2426379789
C,3.1158315149,1.1079281918,-0.0986513548
C,1.6677742767,1.6380267355,-0.1724875509
C,0.5712934666,0.5984060739,0.0662148703
C,-0.8443705743,1.1775068035,-0.0667890159
C,-1.9467074253,0.1410668696,0.1962459213
C,-3.339545413,0.7299398647,0.0370736092
C,-5.6256676104,-0.0179862751,0.2260872464
C,-6.1549807006,1.2338933398,-0.1243697633
C,-6.499634477,-1.0893582095,0.5142333843
C,-7.5393809245,1.3985046483,-0.1840646916
C,-7.870021439,-0.9161543483,0.4529366024
C,-8.4114736415,0.3397707328,0.0997416582
C,-11.9456003099,-0.024335198,0.1603708928
C,-12.8263028408,-1.0709182184,0.4548671416
C,-12.4754435361,1.2295483955,-0.2119254751
C,-14.2108456297,-0.8943235304,0.3872345804
C,-13.8459176129,1.4140013116,-0.2822975523
C,-14.7244184791,0.3545386767,0.0165295329
F,10.6989368621,-1.4420507,0.5928079766
F,9.9840057876,-1.3178120466,-1.594436994
H,4.8501035341,-5.5812647584,0.423839466
H,7.3414783976,-4.4794897489,0.2524150609
H,5.9456679736,0.1384868448,-0.1875047416
H,9.8819441728,2.9614285627,-0.1283913957
H,8.5869291883,5.3637738603,-0.1520676972
H,5.9192490774,4.7512533454,-0.1556716112
H,3.1122406282,-3.4709105288,0.3028581647
H,4.4079552627,-1.380778085,0.0906041697
H,5.6624095565,2.296977217,-0.1336928585
H,1.5493736777,2.0966226767,-1.1645474004
H,1.5852036677,2.464560646,0.5453306053
H,0.7021231322,-0.2304823263,-0.6392131084
H,0.6979402045,0.1612652388,1.0648628359
H,-0.9620706897,2.0197316277,0.631473001
H,-0.970904308,1.5980119235,-1.0757662
H,-1.8382381248,-0.7049104639,-0.4938358418
H,-1.84593238,-0.2631923419,1.2111474184
H,-3.4939719278,1.5651428819,0.7342738434
H,-3.4922477435,1.1009738062,-0.9857745873
H,-5.5059532683,2.0712127783,-0.3489303956
H,-6.0640211392,-2.0467061686,0.7824811651
H,-7.966532674,2.3595692823,-0.4542972095
H,-8.5426569714,-1.7371756332,0.6729923658
H,-12.4082619658,-2.0316570489,0.7396079163
H,-11.7942675025,2.0409791598,-0.4409710418
H,-14.2706131875,2.3715440895,-0.5673025378
H,-14.8661638949,-1.7246656232,0.6215962237
N,4.8758414139,-2.3107878883,0.1511882731
N,6.6031736891,2.7492328211,-0.1334396504
N,-9.787188651,0.6305740996,0.0028338648
N,-10.5680932481,-0.3264381028,0.2638125315
O,8.486815871,-2.0112827597,0.0808676403
O,9.2773730844,0.30471697,-0.0457674623
O,4.0186567838,1.9893527023,-0.1644981332
O,3.2766766488,-0.1399940208,0.0064280874
O,-4.303531061,-0.3010286741,0.3148145338
O,-16.0555905436,0.6461882738,-0.0847054448
C,-16.9994835465,-0.3776159666,0.2026303148
H,-17.9817031625,0.0740080532,0.0575347974
H,-16.8855648306,-1.2292291369,-0.4799021627

H,-16.9080671148,-0.7259237862,1.2391478837

Cartesian Coordination of 2a·*cis*-4′⁻

-2056.534648 hartree

B,-9.1021892385,1.4613463932,-0.318215198
C,-7.4809956889,-1.8798071688,-0.6988815055
C,-7.5944816334,-0.4701593608,-0.425374986
C,-6.4919601766,0.3626346671,-0.2028867854
C,-6.7114817399,1.6905924149,0.1789053646
C,-5.6535705117,2.5943199001,0.5528608899
C,-8.5012723169,-2.7990678685,-0.975332069
C,-7.8919450466,-4.052440245,-1.1774769683
C,-6.5167509393,-3.8630304393,-1.0185278003
C,-3.5890319495,3.3104043719,0.9906172115
C,-4.4441023323,4.3966949055,1.191438066
C,-5.748717982,3.9440812494,0.9146436903
C,-2.7261974151,-1.1929426736,-0.1054012513
C,-1.3161730003,-1.8214605233,-0.1104099848
C,-0.1670371086,-0.8688063688,0.2234154079
C,1.2070261062,-1.5533254946,0.2006890852
C,2.3612727305,-0.595514131,0.5295317062
C,3.7142320476,-1.2891184207,0.5043204846
F,-10.1958699048,1.6781574495,0.5041248619
F,-9.33047676,1.9181738573,-1.61787947
H,-4.1479102532,5.3905629984,1.4984314989
H,-6.6718310357,4.503323848,0.9582555776
H,-5.4861992484,-0.0337692095,-0.2569113904
H,-9.5522809054,-2.5536921702,-1.0202993039
H,-8.3818225363,-4.9875765756,-1.4126076156
H,-5.6970461026,-4.5636950831,-1.0898029282
H,-2.5161240588,3.231336157,1.0929735136
H,-3.8955452274,1.3051469338,0.4056139565
H,-5.3219379671,-2.1807871524,-0.5656953419
H,-1.1689620501,-2.2724900815,-1.1012335137
H,-1.3375703203,-2.663664158,0.5947642023
H,-0.1751274388,-0.0315956317,-0.4852309449
H,-0.3424745877,-0.4231741897,1.2101692492
H,1.2099174316,-2.3891907739,0.9164220104
H,1.3749906918,-2.0003372537,-0.7906645166
H,2.3758508727,0.2333036777,-0.1892328356
H,2.2089323863,-0.1514182419,1.5211087523
H,3.7553135364,-2.0956742278,1.2495993771
H,3.9129104042,-1.7232984198,-0.4855823438
N,-4.3199565864,2.2360918533,0.6090542853
N,-6.2792271206,-2.5612443404,-0.7323596269
O,-7.9257911674,2.1894712247,0.2483518117
O,-8.8231384669,-0.0066974012,-0.3658465468
O,-3.6708677513,-1.9835312196,-0.3861418336
O,-2.8184038444,0.035380896,0.1721461155
O,4.7272594146,-0.3138509622,0.8048572301
C,6.0302688208,-0.6901375625,0.8242769903
C,6.4925883778,-1.9948743257,0.5903592618
C,6.9566784842,0.3276051521,1.125040117
C,7.8607264481,-2.2626449541,0.6619886216
H,5.802178558,-2.8028499925,0.3818070116
C,8.3166150685,0.0614909962,1.1482495322
H,6.5781509016,1.3224212867,1.3367123037
C,8.7902518642,-1.2416639723,0.8926883968
H,8.2260389057,-3.2763685387,0.5266856087
H,9.012321406,0.8593450385,1.3817457743
N,10.1519575859,-1.653890831,1.0365554545
N,11.1429067778,-0.9775669851,0.6702920624
C,11.0599071673,0.1968535975,-0.1481879387
C,11.9293825058,1.247049758,0.1603397593
C,10.3133858558,0.2597537517,-1.3408087928
C,12.0028798265,2.3848193291,-0.6487474145
H,12.5462287958,1.1711415957,1.0508883359
C,10.4110156166,1.3672032121,-2.1706912318
H,9.6649995827,-0.5636687596,-1.6192373526
C,11.241349049,2.4463425437,-1.8227169743
H,12.6666139556,3.1935257284,-0.367065106
H,9.8478507709,1.4223415983,-3.0967328759
O,11.2488831826,3.4946924874,-2.7000130347
C,12.0600909094,4.62380395,-2.4036644988
H,11.8978429567,5.3288997786,-3.2198654396
H,11.7646197951,5.0905912435,-1.4554765116
H,13.1230877934,4.3538937227,-2.3619828769

[S3 (Complete form of ref. 13 in the manuscript)] *Gaussian 09* (Revision D.01), M. J. Frisch, G. W. Trucks, H. B. Schlegel, G. E. Scuseria, M. A. Robb, J. R. Cheeseman, G. Scalmani, V. Barone, B. Mennucci, G. A. Petersson, H. Nakatsuji, M. Caricato, X. Li, H. P. Hratchian, A. F. Izmaylov, J. Bloino, G. Zheng, J. L. Sonnenberg, M. Hada, M. Ehara, K. Toyota, R. Fukuda, J. Hasegawa, M. Ishida, T. Nakajima, Y. Honda, O. Kitao, H. Nakai, T. Vreven, J. A. Montgomery, Jr., J. E. Peralta, F. Ogliaro, M. Bearpark, J. J. Heyd, E. Brothers, K. N. Kudin, V. N. Staroverov, T. Keith, R. Kobayashi, J. Normand, K. Raghavachari, A. Rendell, J. C. Burant, S. S. Iyengar, J. Tomasi, M. Cossi, N. Rega, J. M. Millam, M. Klene, J. E. Knox, J. B. Cross, V. Bakken, C. Adamo, J. Jaramillo, R. Gomperts, R. E. Stratmann, O. Yazyev, A. J. Austin, R. Cammi, C. Pomelli, J. W. Ochterski, R. L. Martin, K. Morokuma, V. G. Zakrzewski, G. A. Voth, P. Salvador, J. J. Dannenberg, S. Dapprich, A. D. Daniels, Ö. Farkas, J. B. Foresman, J. V. Ortiz, J. Cioslowski and D. J. Fox, Gaussian, Inc., Wallingford CT, 2013.

4. Examination of organized structures

Differential scanning calorimetry (DSC). The phase transitions were measured on a differential scanning calorimetry (Hitachi DSC6220).

X-ray diffraction analysis (XRD). Synchrotron XRD measurements of **4**$^{-}$-TBA^{+}, **2a**·**4**$^{-}$-TBA^{+}, and **2b**·**4**$^{-}$-TBA^{+} sealed into quartz capillaries were carried out using a synchrotron radiation X-ray beam (λ = 1.00 Å) on BL40B2 at SPring-8 (Hyogo, Japan). The diffractions were detected a large Debye-Scherrer camera with an imaging plate. The camera lengths were set at 582.7 mm (**4**$^{-}$-TBA^{+}) and 582.0 mm (**2a**·**4**$^{-}$-TBA^{+} and **2b**·**4**$^{-}$-TBA^{+}) and the diffraction patterns were obtained with a 0.01° step in 2θ. An exposure time of the X-ray beam was 10 sec.

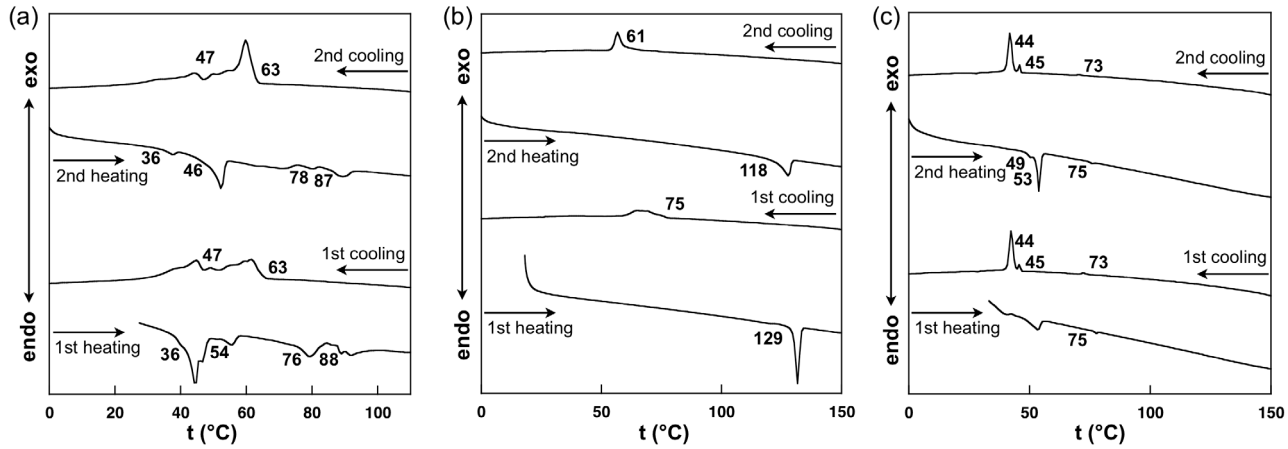

Fig. S7 DSC thermogram (5 °C/min) of (a) **4**$^{-}$-TBA^{+}, (b) **2a**·**4**$^{-}$-TBA^{+}, and (c) **2b**·**4**$^{-}$-TBA^{+}. Onset temperatures (°C) of phase transitions are labeled although some peaks are weak.

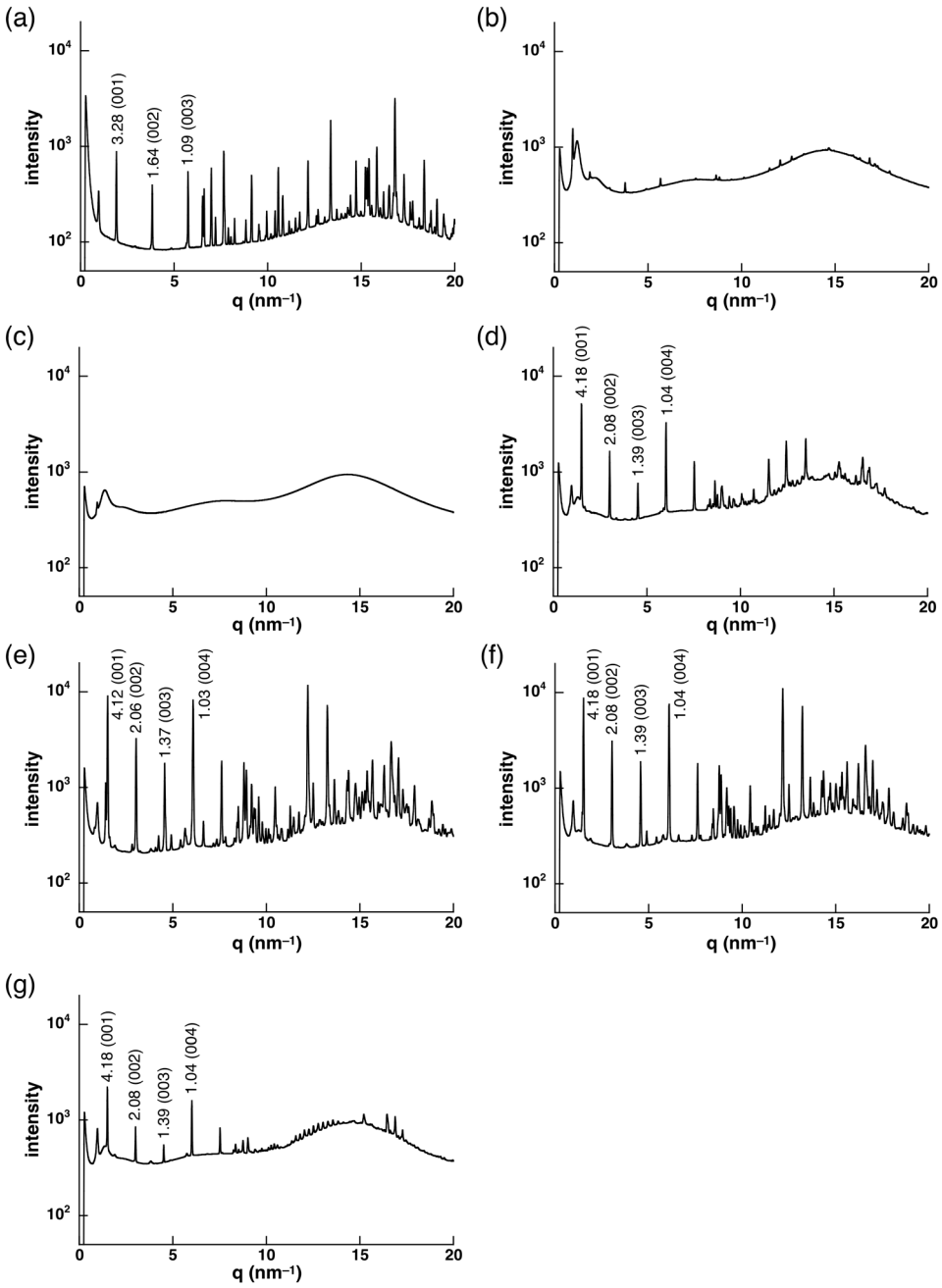

Fig. S8 Synchrotron XRD patterns of $\mathbf{4}^{-}$-TBA^{+} at (a) 25 °C, (b) 70 °C, (c) 100 °C, (d) 60 °C, (e) 20 °C, (f) 50 °C, and (g) 70 °C upon (a–c) 1st heating, (d,e) 1st cooling, and (f,g) 2nd heating. The measurements were performed using a quartz capillary.

Table S1 Synchrotron XRD peaks of **4**$^{-}$-TBA^{+} at (d) 60 °C (1st cooling), (e) 20 °C (1st cooling), (f) 50 °C (2nd heating), and (g) 70 °C (2nd heating). The peaks which can be indexed are represented.

	q (nm^{-1})	*d*-spacing (nm)	ratio	ratio (calc.)	*hkl*
(d) **4**$^{-}$-TBA^{+} 60 °C (1st cooling) lamellar	1.50	4.18	1.0	1.00	001
	3.00	2.08	0.50	0.500	002
	4.50	1.39	0.33	0.333	003
	6.00	1.04	0.25	0.250	004
(e) **4**$^{-}$-TBA^{+} 20 °C (1st cooling) lamellar	1.51	4.12	1.0	1.00	001
	3.02	2.06	0.50	0.500	002
	4.53	1.37	0.33	0.333	003
	6.04	1.03	0.25	0.250	004
(f) **4**$^{-}$-TBA^{+} 50 °C (2nd heating) lamellar	1.50	4.18	1.0	1.00	001
	3.00	2.08	0.50	0.500	002
	4.50	1.39	0.33	0.333	003
	6.00	1.04	0.25	0.250	004
(g) **4**$^{-}$-TBA^{+} 70 °C (2nd heating) lamellar	1.50	4.18	1.0	1.00	001
	3.00	2.08	0.50	0.500	002
	4.50	1.39	0.33	0.333	003
	6.00	1.04	0.25	0.250	004

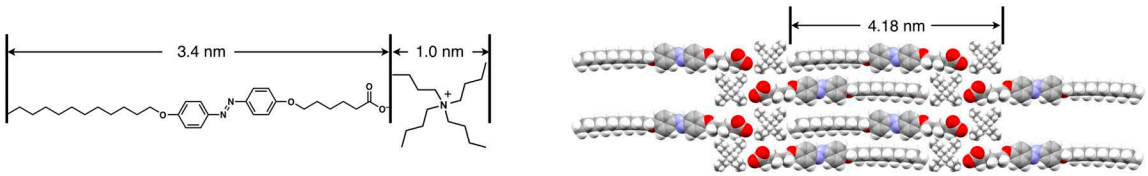

Fig. S9 Chemical structure and schematic illustration of the assembled arrangement in lamellar of **4**$^{-}$-TBA^{+} at 50 °C.

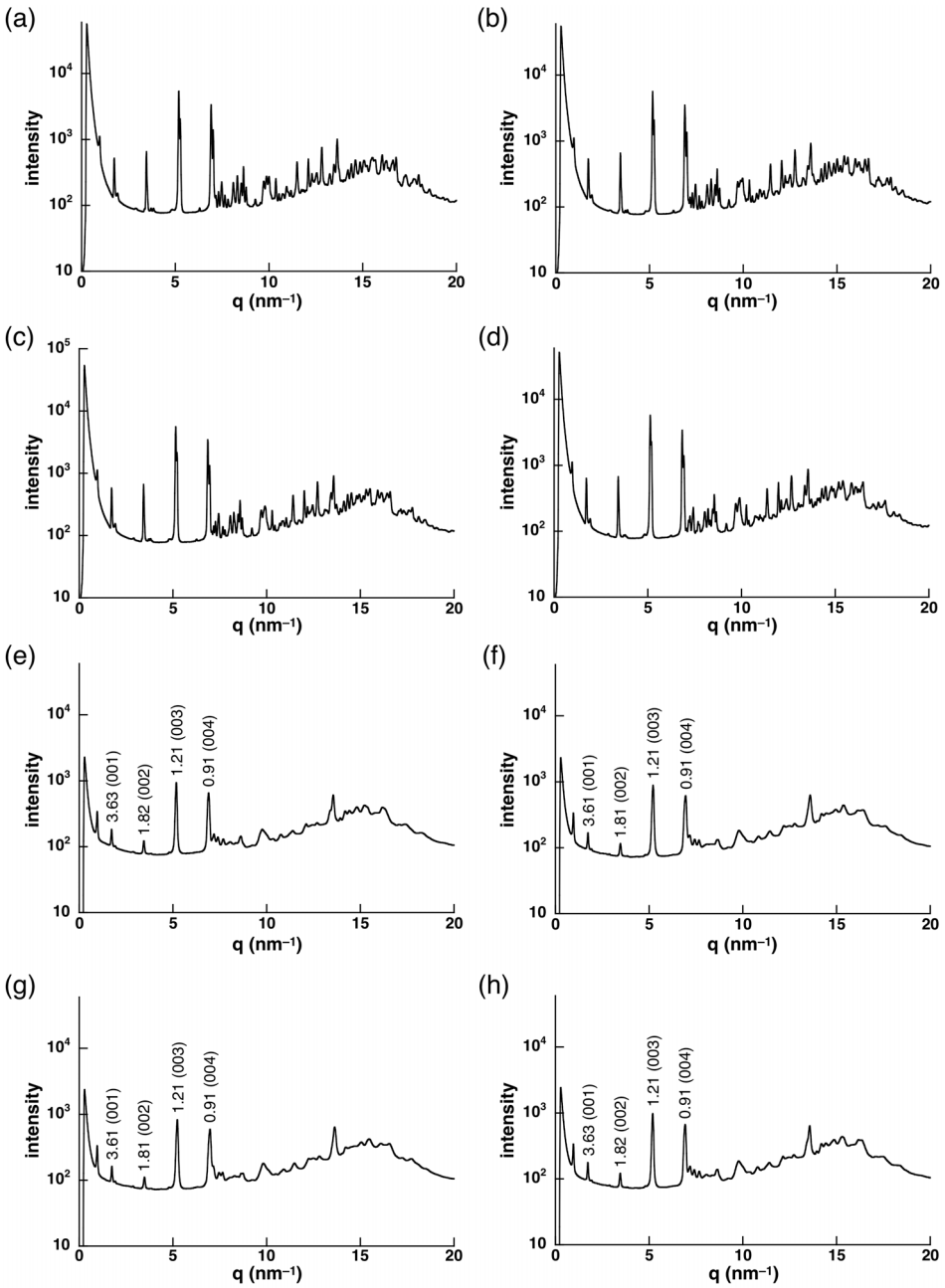

Fig. S10 Synchrotron XRD patterns of **2a**·**4**$^{-}$-TBA^{+} at (a) 25 °C, (b) 50 °C, (c) 70 °C, (d) 90 °C, (e) 80 °C, (f) 50 °C, (g) 25 °C, and (h) 70 °C upon (a–d) 1st heating, (e–g) 1st cooling, and (h) 2nd heating. The measurements were performed using a quartz capillary.

Table S2 Synchrotron XRD peaks of **2a**·**4**$^{-}$-TBA^{+} at (e) 80 °C (1st cooling), (f) 50 °C (1st cooling), (g) 25 °C (1st cooling), and (h) 70 °C (2nd heating). The peaks which can be indexed are represented.

	q (nm^{-1})	*d*-spacing (nm)	ratio	ratio (calc.)	*hkl*
(e) **2a**·**4**$^{-}$-TBA^{+} 80 °C (1st cooling) lamellar	1.72	3.63	1.0	1.00	001
	3.46	1.82	0.50	0.500	002
	5.19	1.21	0.33	0.333	003
	6.92	0.91	0.25	0.250	004
(f) **2a**·**4**$^{-}$-TBA^{+} 50 °C (1st cooling) lamellar	1.73	3.61	1.0	1.00	001
	3.46	1.81	0.50	0.500	002
	5.19	1.21	0.33	0.333	003
	6.92	0.91	0.25	0.250	004
(g) **2a**·**4**$^{-}$-TBA^{+} 25 °C (1st cooling) lamellar	1.73	3.61	1.0	1.00	001
	3.46	1.81	0.50	0.500	002
	5.19	1.21	0.33	0.333	003
	6.92	0.91	0.25	0.250	004
(h) **2a**·**4**$^{-}$-TBA^{+} 70 °C (2nd heating) lamellar	1.72	3.63	1.0	1.00	001
	3.46	1.82	0.50	0.500	002
	5.19	1.21	0.33	0.333	003
	6.92	0.91	0.25	0.250	004

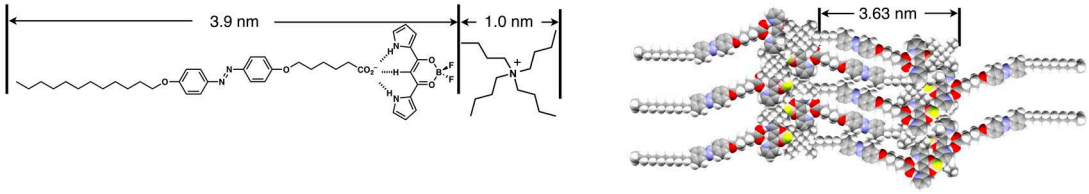

Fig. S11 Chemical structure and schematic illustration of the assembled arrangement in lamellar of **2a**·**4**$^{-}$-TBA^{+} at 25 °C.

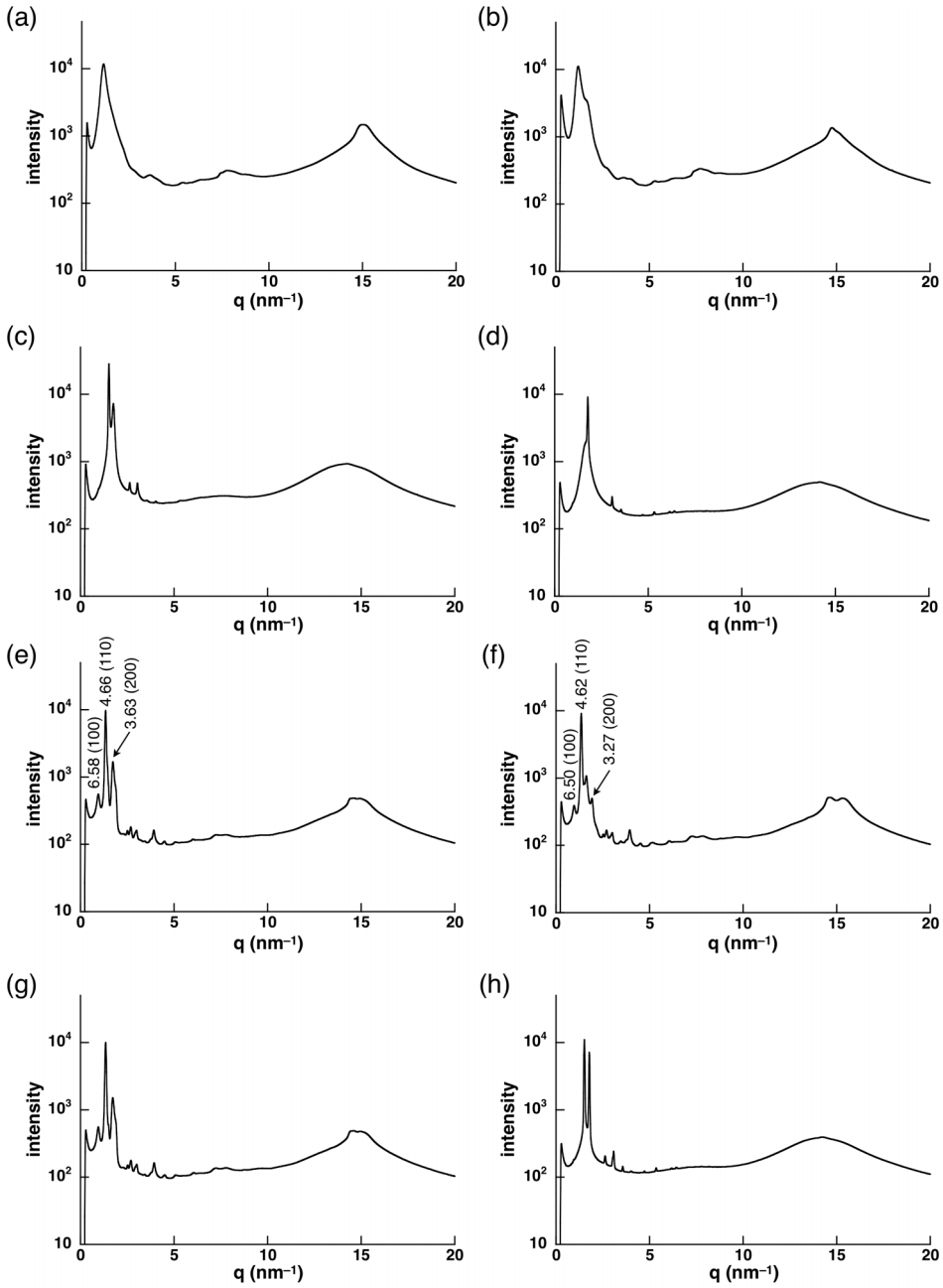

Fig. S12 Synchrotron XRD patterns of **2b**·**4**$^{-}$-TBA^{+} at (a) 25 °C, (b) 50 °C, (c) 70 °C, (d) 100 °C, (e) 50 °C, (f) 20 °C, (g) 50 °C, and (h) 70 °C upon (a–d) 1st heating, (e,f) 1st cooling, and (g,h) 2nd heating. The measurements were performed using a quartz capillary.

Table S3 Synchrotron XRD peaks of **2b**·**4**$^{-}$-TBA^{+} at (e) 50 °C (1st cooling) and (f) 20 °C (1st cooling). The peaks which can be indexed are represented.

	q (nm^{-1})	*d*-spacing (nm)	ratio	ratio (calc.)	*hkl*
(e) **2b**·**4**$^{-}$-TBA^{+}	0.95	6.58	1.0	1.00	100
50 °C (1st cooling)	1.35	4.66	0.71	0.707	110
Col$_t$	1.72	3.63	0.55	0.500	200
a = 6.6 nm					
(f) **2b**·**4**$^{-}$-TBA^{+}	0.97	6.44	1.0	1.00	100
20 °C (1st cooling)	1.36	4.62	0.72	0.707	110
Col$_t$	1.92	3.27	0.51	0.500	200
a = 6.4 nm					

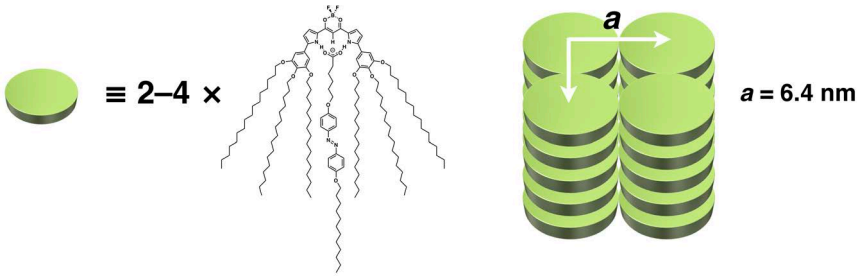

Fig. S13 Chemical structure and schematic illustration of the assembled arrangement in Col_t of **2b**·**4**$^{-}$-TBA^{+} at 20 °C. The locations of cations could not be assigned by XRD measurements.

5. Photo-isomerization properties

Absorption spectroscopy. Variable temperature UV-visible absorption spectra for film of **2b**·**4**$^{-}$-TBA^{+} were measured by Ocean Optics QE6500 spectrometer/DH-2000-BAL light source system equipped with an Ocean Optics QR450-7-XSR reflection fiber probe. A mirror was placed at the bottom of a temperature-controlled stage (Mettler-Toledo FS-32/FP-90 system). The probing light passed the film samples and was reflected by the mirror. The UV irradiation (365 nm) of the film samples was performed using Asahi-Spectra REX-250 super high-pressure mercury lamp with appropriate bandpass filters.

Polarizing optical microscopy (POM). Birefringent changes in photo-induced phase transitions were evaluated with an optical microscope under a crossed polarizer condition using an Olympus BX51-FL fluorescence microscope equipped with a Nikon DS-Ri2 digital camera. The actinic UV light (365 nm) for the photo-isomerization was irradiated by a mercury lamp with fluorescence mirror units (U-MNU2). A sandwiched cell (8-μm spacer) was placed on the temperature-controlled stage. The texture of the sample was observed through a set of crossed polarizer and analyzer.

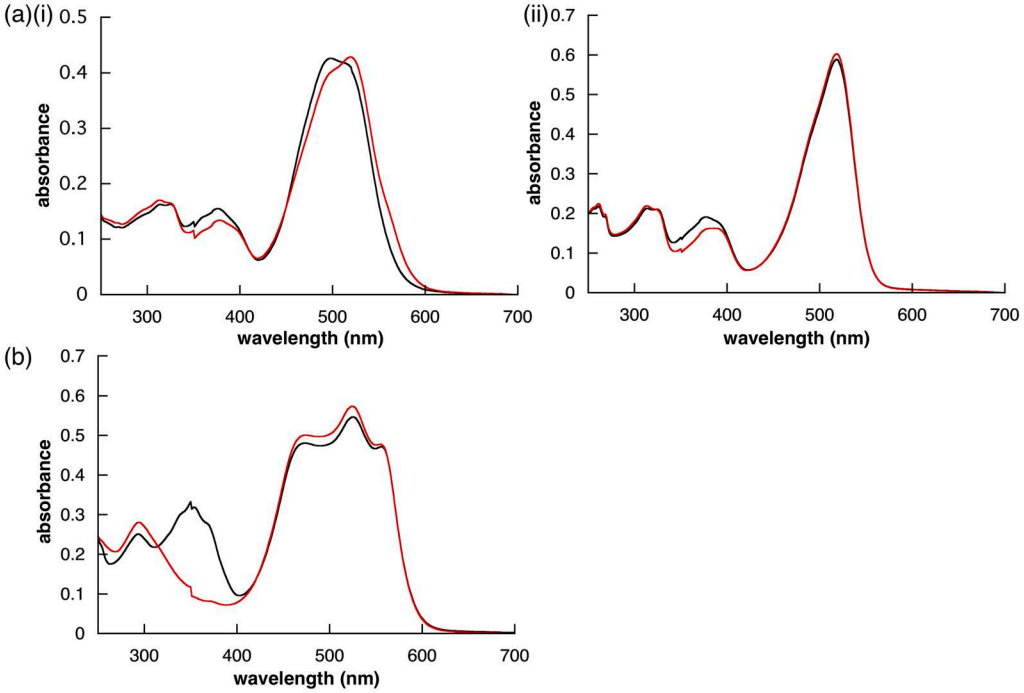

Fig. S14 UV/vis absorption spectral change of (a) **2b**·**4**$^{-}$-TBA^{+} (3.9 mM and 1.0 mM for (i) and (ii), respectively) and (b) the 1:1 mixture of **2b** and **3** (4.0 mM) in *n*-octane at rt. Black and red lines indicate before and after UV irradiation (365 nm). Before the UV irradiation, the absorption band of **2b**·**4**$^{-}$-TBA^{+} in the long-wavelength region became broad and shifted from 520 nm to 479 nm by increasing concentrations, indicating the formation of the aggregation. After the UV irradiation, the absorption band at 376 nm decreased, while that at 479 nm concurrently shifted to 520 nm, indicating that disaggregation of the π-electronic system occurred upon conformation change of azobenzene from *trans* to *cis* forms, because the absorption spectrum in the long-wavelength region after photoirradiation was similar to that in a diluted solution without aggregation.

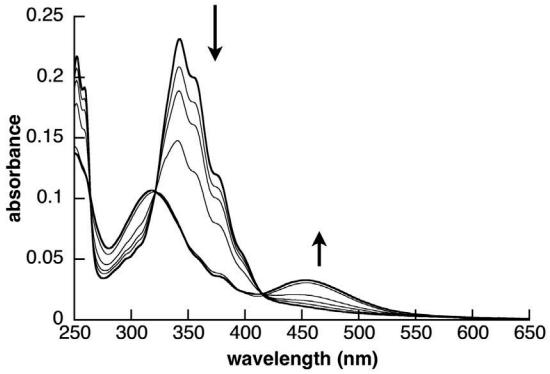

Fig. S15 UV/vis absorption spectral change of **4**$^{-}$-TBA^{+} under UV irradiation (365 nm) at rt in spin-coated film.

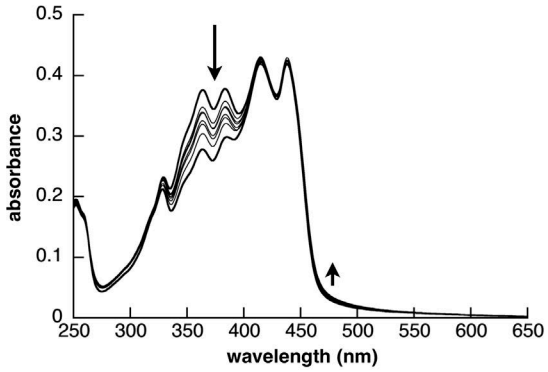

Fig. S16 UV/vis absorption spectral change of **2a**·**4**$^{-}$-TBA^{+} under UV irradiation (365 nm) at rt in spin-coated film.

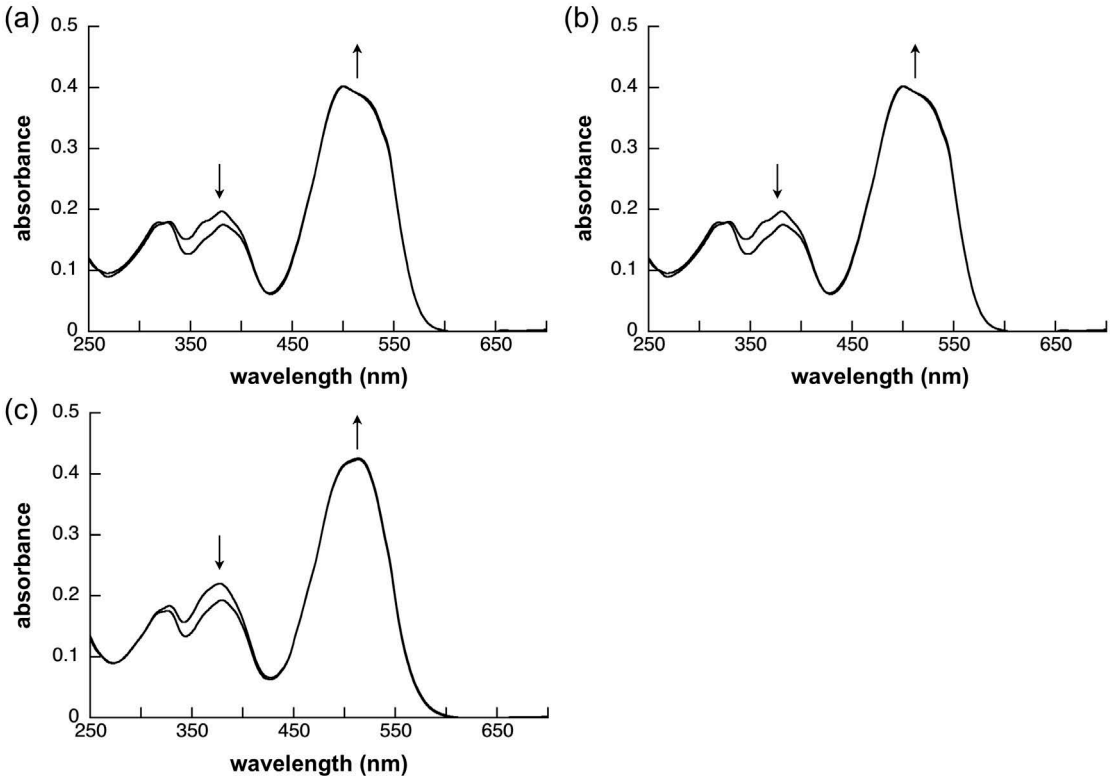

Fig. S17 UV/vis absorption spectral change of **2b**·**4**$^{-}$-TBA^{+} under UV irradiation (365 nm, 200 mW/cm^2) at (a) 25 °C, (b) 50 °C, and (c) 100 °C in thin film.

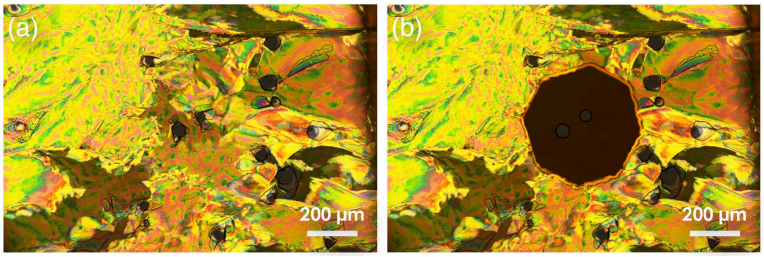

Fig. S18 Photo-induced phase transition of **4**$^{-}$-TBA^{+} in a sandwiched cell (8-µm spacer) observed by POM under UV irradiation (central spot, 365 nm, 200 mW/cm^2) at 50 °C: (a) initial state and (b) after 1 min.

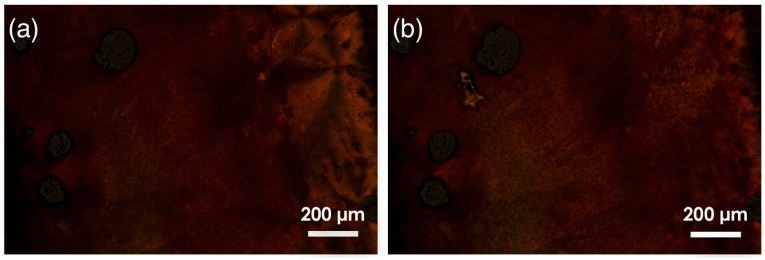

Fig. S19 Photo-induced phase transition of **2a**·**4**$^{-}$-TBA^{+} in a sandwiched cell (8-µm spacer) observed by POM under UV irradiation (central spot, 365 nm, 200 mW/cm^2) at 90 °C: (a) initial state and (b) after 5 min.

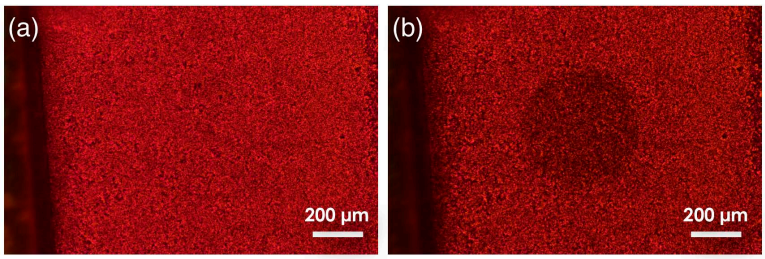

Fig. S20 Photo-induced phase transition of **2b**·**4**$^{-}$-TBA^{+} in a sandwiched cell (8-µm spacer) observed by POM under UV irradiation (central spot, 365 nm, 200 mW/cm^2) at 70 °C: (a) initial state and (b) after 5 min.